250 kV Sub-nanosecond Pulse Generator with Adjustable Pulse-width

Tammo Heeren, J. Thomas Camp, Juergen F. Kolb, Karl H. Schoenbach
Frank Reidy Research Center for Bioelectrics
Old Dominion University
Norfolk, VA 23510, USA

Sunao Katsuki and **Hidenori Akiyama**
Department of Electrical Engineering
Kumamoto University
Kumamoto 860, Japan

ABSTRACT

This paper details the construction of a sub-nanosecond pulse generator capable of delivering 250 kV into a high impedance load. The pulse width is approximately 600ps with a voltage rise of up to 1 MV/ns. The pulse rise-time can be adjusted by manipulation of a peaking gap, whereas the pulse-width can be changed by adjusting a novel tail-cut switch located close to the load.

Index Terms — **Pulse generation, Marx generators.**

1 INTRODUCTION

TRADITIONALLY, pulse generators for the investigation of the effects of nanosecond pulsed electric fields (nsPEF) on cells have used pulse-widths in the range of 3-300 ns [1-3]. An overview of various technologies employed in generating these pulses is given in [4]. As typical with these pulsers, the load is a given volume of biological cells in suspension. However, the application of these pulses to in vivo tissues is limited to superficial body tissues. To target deeper tissues, it would be of great benefit to be able to focus the electric field of an impulse-radiating antenna (IRA) such as is presented in [5]. To obtain reasonable spatial resolution, this would require extremely short (subnanosecond) pulses. To evaluate the possibility of causing any desired effects in tissues and cells with PEF of less than 1 ns, we constructed the pulse generator previously introduced in [6] and discussed in more detail here.

2 SYSTEM OVERVIEW

Figure 1 shows the conceptional arrangement of the subnanosecond pulse generator utilized for the exposure of biological cell in suspension to sub-nanosecond pulsed electric fields (PEFs) with field strength as high as 0.8 MV/cm. The pulser is comprised of six different sections: power supply, pulse generator, peaking circuit, transmission line, tailcut switch, and exposure chamber. Each of these sections will be discussed in the following.

Manuscript received on 22 November 2006, in final form 16 March 2007.

2.1 POWER SUPPLY

The power supplies used to charge the pulse generator and the transmission-line type trigger generator are standard 20 kV high-voltage power supplies.

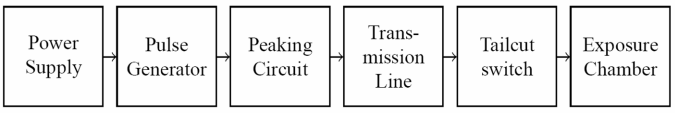

Figure 1. Conceptional layout of the sub-nanosecond pulse generator.

2.2 PULSE GENERATOR

The pulse generator is an improved waveguide Marx generator with 20 stages [7]. The stray capacitance was reduced to increase the output voltage and pulse rise-time. Each stage has a capacitance of Cs = 500 pF. The size of the individual charging resistors was guided by the requirement to operate the generator at a frequency of approximately f = 10 Hz. The charging time constant of the last (N^{th}) capacitor is given by $\tau_c = \alpha R_s C_s N^2$, where $\alpha = 0.9$ yields a good match. Similar relationships (with $\alpha = 1$) are published in [7,8]. Thus, to charge the last stage to 99.3%, e.g. ($1\text{-}e^{-5}$), within T = 100 ms, the maximum stage resistance R_s is given by

$$R_s \le \frac{T}{5\alpha C_s N^2} = \frac{100\ ms}{5.0.9 \times 400\ \times 500\ pF} = 111\ k\Omega \qquad (1)$$

A value of R_s = 100 kΩ was chosen. Provided that all energy is transferred to the load, the maximum dissipation of

any resistor in the generator is less then 3 W for 10 Hz operation. If no energy is dissipated in the load, but the Marx generator has erected, the stage resistors have to dissipate an additional 0.5 W. The breakdown voltage of the individual spark-gap switches is adjusted by pressurizing the entire Marx generator to 700 kPA (≈100 psi) with dry air. The moisture content of the air is further reduced to approximately 25 ppb with the help of a moisture trap to reduce spark-gap contamination and erosion.

2.3 PEAKING CIRCUIT

Peaking capacitors are frequently employed in Marx generators to decrease the rise-time of the pulse. It essentially provides a fast RLC circuit to drive the rising edge of the pulse. It is imperative to keep this circuit from ringing [9]. Figure 2 details the geometry of the peaking capacitor. It is used to decrease the rise-time of the output pulse by reducing the effective discharge inductance. With the help of finite-element software [10,11], the peaking capacitance C_P was estimated to be approximately 4 pF. Figure 3 and figure 4 show the dependence of the pulse rise-time on the electrode separation. A distance of 0 mm indicates that the electrodes are in contact and no peaking effect occurs. The voltage trace therefore shows the pulse rise-time of the Marx generator (solid trace). Once the gap distance is increased the pulse breakdown occurs at a later time but with a faster rise. The voltage rise at the load is 380 kV/ns, 600 kV/ns, and 1 MV/ns for gap separations of 0.85 mm, 1.35 mm, and ≥ 2.7 mm respectively.

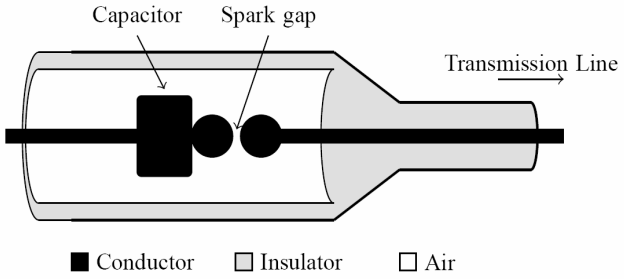

Figure 2. Diagram detailing the peaking circuit used to decrease the pulse rise-time.

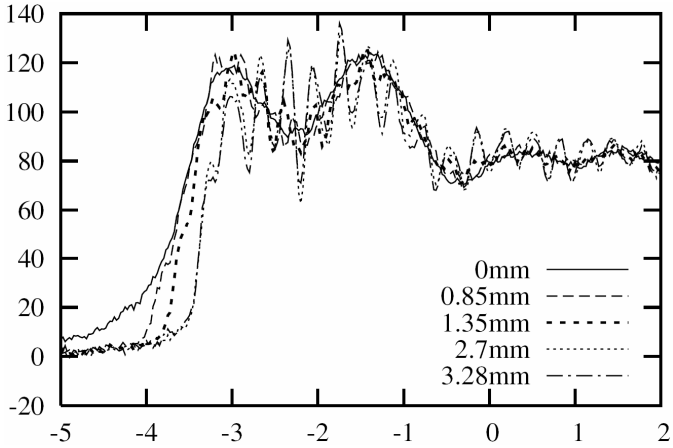

Figure 3. Voltage for different separations of the peaking gap measured with a capacitive voltage probe (probe 2, see chapter 3). Abscissa in ns, Ordinate in kV.

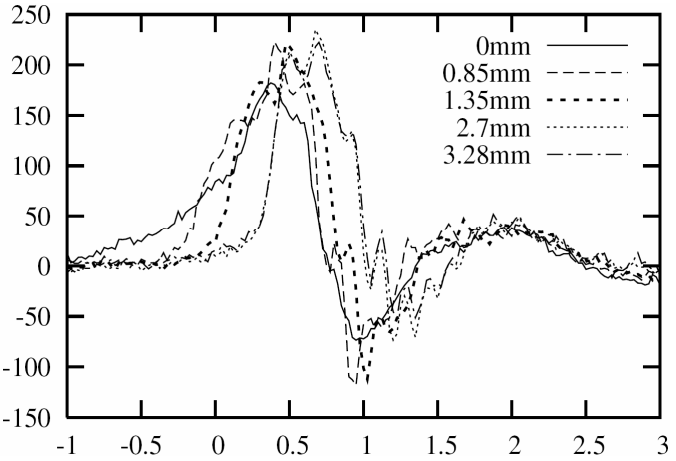

Figure 4. Chamber probe (Probe 1) voltage for different separations of the peaking gap. Abscissa in ns, Ordinate in kV

2.4 TRANSMISSION LINE

The transmission line employed to deliver the pulse to the exposure chamber is an RG220/U with a published $\varepsilon_r = 2.275$ and an impedance of 50 Ω.

2.4 EXPOSURE CHAMBER AND TAIL-CUT SWITCH

The design of the exposure chamber for cells in suspension is illustrated in Figure 5. It has a coaxial arrangement with the transmission line cable entering from the bottom. The shielding of the transmission line is connected to the return conductor (housing), which, in turn, is grounded. The capacitance $C_{chamber}$ of the exposure volume is estimated to be 4.25 pF · mm. The tail-cut switch is located close to the exposure chamber (5.7cm from the center of the exposure chamber to the tail-cut switch). It essentially is a small hole in the dielectric with a diameter of approximately 1 mm in the dielectric (see Figure 6). The exposure chamber itself is cylindrical with polished stainless steel electrodes on both ends. The electrodes are larger than the diameter of the volume to ensure a homogeneous field within the chamber. While the diameter of the chamber is fixed to 2.75 mm, its height is variable to allow for different electric field strengths. We employed four different chambers with heights of 3.15 mm, 3.91 mm, 5.35 mm, and 10.67 mm height.

3 VOLTAGE MEASUREMENT AND PROBE CALIBRATION

In order to measure the voltage (electric field) applied to the sample, two capacitive voltage dividers were installed in the system. One probe (Probe 1) was part of the exposure chamber setup (see figure 5), the other probe (Probe 2) was installed approximately 0.71 m, or 3.9 ns ahead of the previous probe. The probe located close to the sample allows the direct measurement of pulse-width, and amplitude, whereas the second probe can also be used to measure the reflection coefficient of the load. The second coaxial divider (Probe 2) was designed such that, if operated directly into a 50 Ω transmission line, its droop would be less than 2% within 1 ns. The divider uses the full circumference of the coaxial

cable, utilizes a 25 µm Kapton (polyimide) film as dielectric, and has a width of 1.27 cm. These parameters should yield a divider ratio of approximately 850:1. Details about capacitive voltage dividers can be found in [12-14]. Theoretically, the attenuation of a coaxial capacitive divider is solely determined by its geometrical arrangement. However, since small variations in the thickness of the dielectric can cause a drastic change in attenuation, the ratio has to be verified with a pulse of known amplitude. Although not strictly necessary, the calibration pulse should also have a pulse-width that is comparable to the pulse to be measured. For this purpose we constructed a short cable pulser of approximately 9 cm length to give a pulse-width of $\tau = 2l\sqrt{\varepsilon_r}/c = 0.9$ ns. The cable pulser was charged to 1 kV to yield a pulse-amplitude of 500 V into the transmission line leading to the exposure chamber. Measurements with the transmission line terminated with R = 50 Ω (matched), R → 0 (short), R → ∞ (open), and a typical load were performed. The results for the matched, short, and open case are shown in figure 7. The result for the typical load case – a physiological buffer between cylindrical electrodes of 2 mm diameter and a gap distance of 10.67 mm - is shown in figure 8. For each evaluation, the chamber geometry did not change; we simply replaced the exposure volume with water (open), copper (short), a 50 Ω resistor (matched), and cell-suspension (load). From the measurements with a shorted load we can see that the voltage probe is not located exactly at the point of reflection. The short peaks show that the wave travels past the probe before it gets reflected, and before it cancels at the probe on its way back. The same occurs for the trailing end of the pulse with reverse polarity. Furthermore, we can derive from the measurements that the divider ratio of Probe 1 is approximately 770:1, and that of Probe 2 is 425:1 (excluding the two 20 dB attenuators). The effective divider ratio of Probe 2 is about 1/2 the calculated value. Due to the fact that the divider ratio of Probe 1 is likely to change whenever the exposure chamber is changed, Probe 2 can serve as a calibration standard since it is permanently installed on the cable. From the measurement of the amplitudes of the incoming V_{inc} and reflected waves V_{ref} of the load measurement in figure 8, we can calculate the impedance of the load for our typical application. From time-domain reflectometry (TDR) we know that

$$Z_{load} = \frac{V_{inc} + V_{ref}}{V_{inc} - V_{ref}} Z_0 = \frac{11.5 + 7}{11.5 - 7} 50\Omega \approx 200\Omega \qquad (2)$$

where Z_0 is the impedance of the transmission line. Therefore, for our typical application (cells in suspension), we can expect a voltage increase at the load of (200-50)/(200+50) ≈ 0.6.

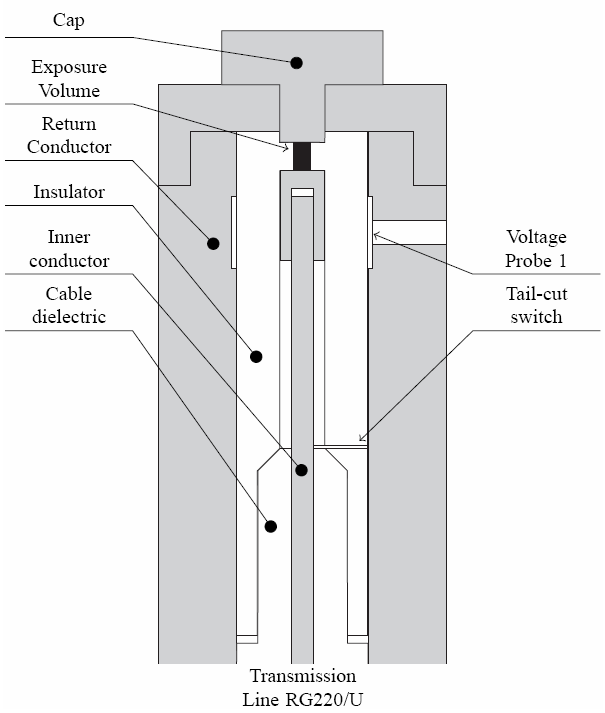

Figure 5. Diagram detailing the exposure chamber. Gray: conductor, White: insulator, Black: load. The overall diameter is 5.7cm, and the overall height is 12.5cm.

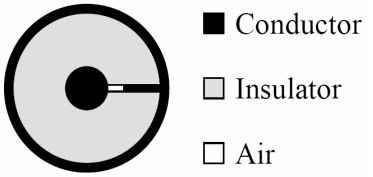

Figure 6. Cross-section of tail-cut switch. Black: conductor, Gray: Insulator, White: air. The diameter is about 2.5cm.

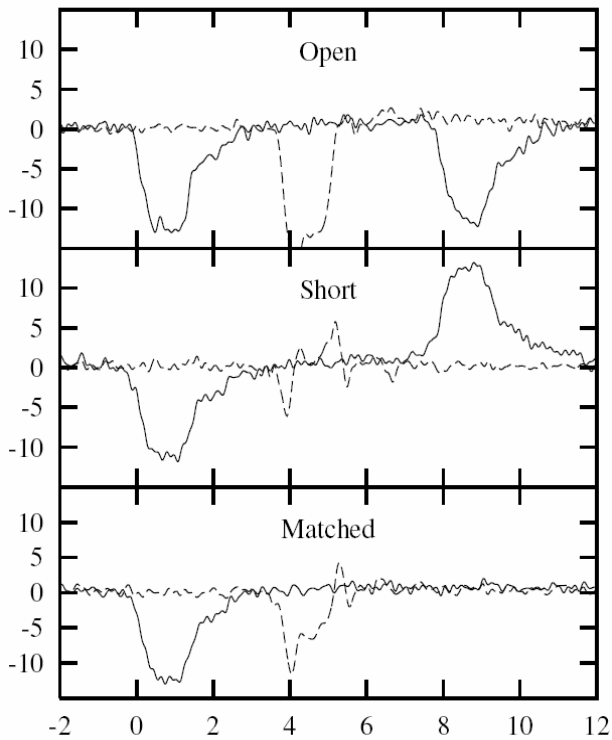

Figure 7. Set of low voltage calibration measurements for three conditions. Abscissa in ns, Ordinate in kV. Dashed traces: Probe 1, Solid traces: Probe 2.

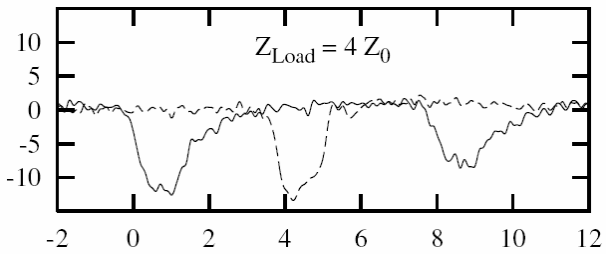

Figure 8. Low voltage measurements of load. Abscissa in ns, Ordinate in kV.

4 VERIFICATION OF TAIL-CUT SWITCH OPERATION

The pulse produced by the pulse generator is sufficiently long compared to the output pulse-width to essentially be considered constant. When the pulse arrives at the tail-cut switch it initiates a breakdown. However, the formation time of the breakdown is sufficiently long to allow the wave to travel toward the load. Once the reflected wave that is superimposed onto the incoming wave arrives at the tail-cut switch, if the load resistance is large compared to the cable impedance, it will approximately double the voltage across it, and finalize the breakdown. Therefore the pulse-width is determined by two parameters: the formation time of the breakdown and the two-way transit time from breakdown to load. That the introduced tail-cut switch performs as expected can be seen in Figures 9 and 10. During low voltage calibration it was shown that both voltage probes deliver signals with comparable pulse width. However, during high voltage operation, the probe located near the load shows a significantly shorter pulse than the probe installed on the cable. From the calibration we also know that the round-trip time probe-load-probe is about 8 ns, whereas in the high-voltage evaluation it is closer to 9 ns. The only possible conclusion is that the tail-cut switch, which is located ahead of probe 1, shortens the pulse after a delay of approximately 1 ns before it hits probe 1. Since probe 2 is located before the tail-cut switch, it will show a pulse that has a pulse-width that is a combination of the round-trip time and the delay time, e.g. 8 ns + 1 ns = 9 ns. Initially it was assumed that a larger diameter of the hole would cause a reduction in the resistive phase of the breakdown due to a decrease in recombination losses at the wall. However, Figure 10 shows that the hole-diameter does not make any significant difference (thin lines), whereas the penetration depth of the tail-cut switch has a significant impact on pulse-width and pulse amplitude (bold lines). The traces shown are averages of 16 individual measurements.

5 RESULTS

Figure 11 shows the output voltages measured with Probe 1 (the probe located closest to the exposure chamber). The peak amplitude is about 250 kV, with a pulse-width of approximately 600 ps. Considering the four different chamber heights, 3.15 mm, 3.91 mm, 5.35 mm, and 10.67 mm, the average electric fields for 250 kV output voltage are 800 kV/cm, 640 kV/cm, 470 kV/cm, and 230 kV/cm, respectively. The pulse duration is obviously determined by the tail-cut switch, as shown in figure 10, where a reduction in the length of the switch gap caused a reduction in pulse duration. However, pulse rise and fall times seem to be influenced by the load capacitance, in this case by the height of the exposure chamber. The pulse will widen for shorter chambers since more energy is stored. The equivalent capacitance that the exposure chamber presents to the pulser ranges from 1.35 pF for the shortest chamber to 0.4 pF for the largest. This corresponds to a maximum RC charging and discharging time constant of 50 Ω 1.35 pF = 67.5 ps, a value which is in the range of the measured rise time of the pulse. For large load resistances, R is the cable impedance, C is the load capacitance. Since the rise time seems to be independent of the load capacitance (figure 11), it is likely limited by our voltage diagnostic to approximately 100 ps. The fall time, however is longer, and seems to be determined by the resistance of the load and that of the tail-cut switch. Since after switch closing the pulse bounces - at a frequency beyond the temporal resolution of our diagnostic circuit - between a high resistance RC circuit (load) and a low resistance tail-cut switch, the energy is dissipated with a time constant longer than the RC time constant, mentioned above.

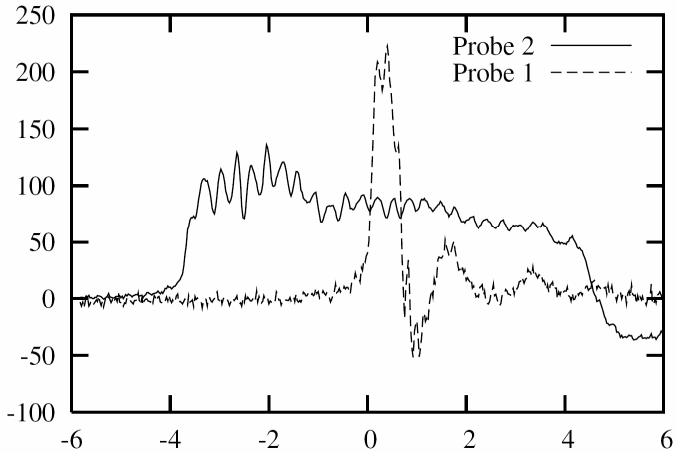

Figure 9. Voltage waveforms of probe 1 (dashed) and probe 2 (solid) for typical operation. Abscissa in ns, Ordinate in kV.

6 SUMMARY

We presented a pulse generator capable of delivering up to 250 kV into a high impedance load with a peak rate-of-voltage increase of 1 MV/ns. The voltage rise is a function of electrode separation in the peaking gap, whereas the pulse-width can be changed by adjusting a novel tail-cut switch located closely to the load. We showed that the rise-time of the pulse can be varied by adjusting the gap distance of the peaking gap, and that the pulse-width can be changed by adjusting the penetration depth of the tail-cut switch. The work discussed here is part of a larger effort to evaluate the possibility of exposing in vivo tissue to nsPEFs without the use of needles and/or plate electrodes. The ps pulse-width of PEFs generated by conical antennas with two focal points will be in

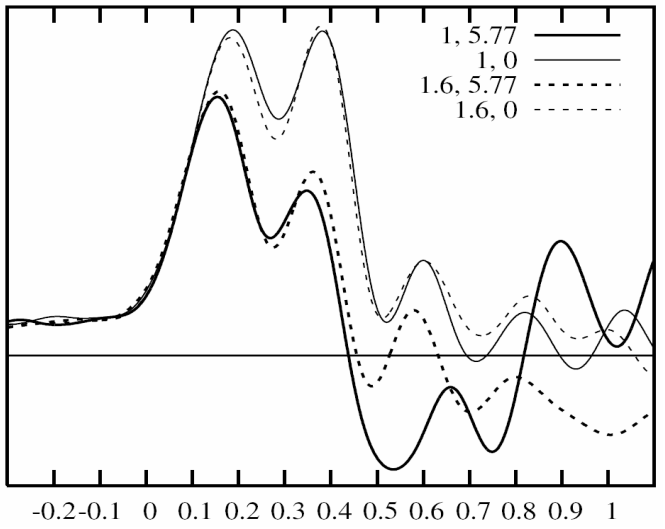

Figure 10. Effect of changing hole diameter and penetration distance. First number: hole diameter in mm, second number: penetration distance in mm. Output of probe 1. Abscissa in ns. Average of 16 traces.

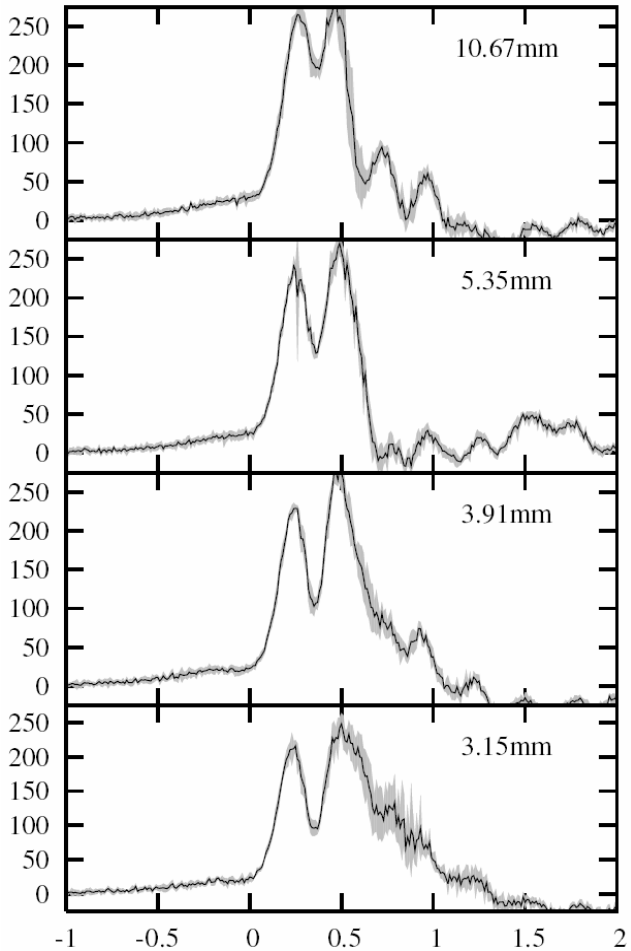

Figure 11. Output voltage measured with Probe 1 (solid) operation with cell suspension (buffer) load for chambers with 3.15 mm, 3.91 mm, 5.35 mm, and 10.67 mm height. Abscissa in ns, Ordinate in kV. Equivalent electric field strengths are 800 kV/cm, 640 kV/cm, 470 kV/cm, and 230 kV/cm respectively. The shaded area indicates the standard deviation margin for each voltage measurement.

the range of ≤ 1 ns. Until now, no evaluation of the effects of PEFs in these time ranges had been performed. The system presented here will yield results as to what electric field strength is necessary to cause desired effects. A possible antenna setup which utilizes a prolate spheroidal IRA as detailed in [15] will be presented in a later paper.

ACKNOWLEDGMENT

This work is supported by Bioelectrics, Inc. and by an Air Force Office of Scientific Research Multidisciplinary University Research Initiative (MURI) grant on subcellular response to narrow-band and wide-band radio frequency radiation, administered through Old Dominion University.

REFERENCES

[1] K. Schoenbach, R. Joshi, J. Kolb, N. Chen, M. Stacey, P. Blackmore, E. Buescher, and S. Beebe, "Ultrashort electrical pulses open a new gateway into biological cells", Proc. IEEE, Vol. 92, pp. 1122-1137, 2004.

[2] K. Schoenbach, F. Peterkin, I. Alden, R.W., and S. Beebe, "The effect of pulsed electric fields on biological cells: experiments and applications", IEEE Trans. Plasma Sci., Vol. 25, pp. 284-292, 1997.

[3] P. T. Vernier, Y. Sun, and M. Gundersen, "Nanoelectropulse-driven membrane perturbation and small molecule permeabilization", BMC Cell Biology, Vol. 7, p. 37, 2006

[4] T. Heeren, J. F. Kolb, S. Xiao, K. H. Schoenbach, and H. Akiyama, "Pulsed power generators and delivery devices for bioelectrical applications", Power Modulator Symposium, 2006 and 2006 High-Voltage Workshop. Conf. Record of the Twenty-Seventh International, 2006, 015.

[5] C. E. Baum, "Producing large transient electromagnetic fields in a small region: an electromagnetic implosion", Sensor and Simulation Notes, Note 501, 2005.

[6] K. H. Schoenbach, S. Katsuki, C. Osgood, T. Heeren, U. Pliquett, J. F. Kolb, R. P. Joshi, and S. J. Beebe, "Biological effects of intense subnanosecond electrical pulses", Power Modulator Symposium, 2006 and 2006 High-Voltage Workshop. Conf. Record of the Twenty-Seventh International, 2006, 016.

[7] W. Carey and J. Mayes, "Marx generator design and performance", in Power Modulator Symposium, 2002 and 2002 High-Voltage Workshop. Conference Record of the Twenty-Fifth International, pp. 625-628, 2002.

[8] J. F. Francis, "High voltage pulse techniques", Pulsed Power Lecture Series, Plasma Laboratory, Texas Tech University, 1976.

[9] S. T. Pai and Q. Zhang, *Introduction to High Power Pulse Technology*, ser. Advanced series in electrical and computer engineering. Singapore; River Edge, N.J., USA, World Scientific, 1995.

[10] P. Dular and C. Geuzaine, "GetDP: a general environment for the treatment of discrete problems," http://www.geuz.org/getdp/.

[11] C. Geuzaine and J.-F. Remacle, "Gmsh: a three-dimensional finite element mesh generator with built-in pre- and post-processing facilities," http://www.geuz.org/gmsh/.

[12] W. Pfeiffer, Impulstechnik, ser. Studienbuecher der technischen Wissenschaften. Carl Hanser Verlag Muenchen Wien, Vol. 94, 1976.

[13] W. Pfeiffer, "Aufbau und Anwendung kapazitiver Spannungsteiler extrem kurzer Ansteigszeit f¨ur gasisolierte Koaxialsysteme", ETZ-A, Vol. 94, pp. 91–94, 1973.

[14] J. E. Thompson and L. H. Luessen, Eds., *Fast Electrical and Optical Measurements*, ser. NATO ASI series (Advanced Study Institute on Fast Electrical and Optical Diagnostic Principles and Techniques). Martinus Nijhoff, 1986.

[15] C. E. Baum, "Focal waveform of a prolate spheroidal IRA", Sensor and Simulation Note 509, February 2006.